archives
of thermodynamics
Vol. **41**(2020), No. 2, 65–83
DOI: 10.24425/ather.2020.133622

Thermal analysis of a gravity-assisted heat pipe working with zirconia-acetone nanofluids: An experimental assessment

AMIN ABDOLHOSSEIN ZADEH[a]
SHIMA NAKHJAVANI[b*]

[a] School of Engineering, University of South Australia, SA 5000, Australia

[b] School of Engineering, University of Yazd, Safaeih, Yazd Province, Iran

Abstract An experimental investigation was performed on the thermal performance and heat transfer characteristics of acetone/zirconia nanofluid in a straight (rod) gravity-assisted heat pipe. The heat pipe was fabricated from copper with a diameter of 15 mm, evaporator-condenser length of 100 mm and adiabatic length of 50 mm. The zirconia-acetone nanofluid was prepared at 0.05–0.15% wt. Influence of heat flux applied to the evaporator, filling ratio, tilt angle and mass concentration of nanofluid on the heat transfer coefficient of heat pipe was investigated. Results showed that the use of nanofluid increases the heat transfer coefficient while decreasing the thermal resistance of the heat pipe. However, for the filling ratio and tilt angle values, the heat transfer coefficient initially increases with an increase in both. However, from a specific value, which was 0.65 for filling ratio and 60–65 deg for tilt angle, the heat transfer coefficient was suppressed. This was attributed to the limitation in the internal space of the heat pipe and also the accumulation of working fluid inside the bottom of the heat pipe due to the large tilt angle. Overall, zirconia-acetone showed a great potential to increase the thermal performance of the heat pipe.

Keywords: Heat pipe; Zirconia-acetone nanofluid; Tilt angle; Filling ratio

*Corresponding Author: Email: shimaa.nakhjavani@gmail.com

1 Introduction

With a continuous progress in microelectronic devices and also with an anomalous advancement in the design and fabrication of the processors and integrated circuits, the rate of heat dissipation from such devices has been increased significantly [1]. Lack of efficient cooling systems together with the capability to remove a large amount of heat from a heat source has led to a limitation in design and fabrication of high-frequency processors and microelectronic integrated circuits. Thereby, much effort has been made to develop and use new systems for cooling the high heat flux chipsets [2,3]. The effort includes but is not limited to liquid cooling loops, piezoelectric, fan coolers and heat sinks, which all have their advantages and drawbacks. For a decade, the plausible application of heat pipes has been the matter of research and various types of heat pipes with different working fluids have been tested with the hope to solve the challenge of heat transfer limitation in cooling systems.

Heat pipes are small devices with the ability to transfer a large amount of heat from a heat source to a cold environment thanks to the phase change phenomena. Generally, the heat pipe has three main sections including evaporator, adiabatic region and a condenser. In the evaporator, the working fluid inside the heat pipe is evaporated by absorbing a large amount of heat including sensible and latent heat, while delivering the heat to environment in the condenser [4–8]. The working fluid is condensed to liquid and returns to the evaporator. Hence, most of heat pipes does not need any external forces to drive the working fluid.

Gravity-assisted heat pipes are devices using gravity to facilitate returning the working fluid to the evaporator. In a gravity-assisted heat pipe, the heat transfer coefficient of evaporator together with the amount of the working fluid are key parameters affecting the overall thermal performance of the heat pipe. To increase the heat transfer coefficient of the evaporator, one potential option is to operate a heat pipe in nucleate boiling heat transfer region. This heat transfer mechanism can provide better heat and mass transfer due to the bubble formation and local agitation of working fluid inside the evaporator section. However, conventional coolants such as water, ethylene glycol or oils have low thermal conductivity, which limits their thermal performance even in the boiling region. One plausible option is to use nanofluids which have been proved to represent better thermal performance and heat transfer characteristics when compared to the current coolants [9]. Nanofluids have various applications in medical

treatments [10-14], and engineering fields [15-18]. A nanofluid is a working fluid comprising a base fluid (conventional coolant, e.g., water) with some conductive solid particles which are uniformly dispersed within the base fluid [19].

Investigations on nanofluids have revealed that a nanofluid has a higher thermal conductivity, heat capacity and sometimes high viscosity and density in comparison with the base fluid. Therefore, using nanofluids brings tangible benefits to the process while also suffers from some disadvantages such as pressure drop, pumping power augmentation and also instability [20,21]. Therefore, many experiments have been conducted to identify a plausible nanofluid to be employed in heat transfer systems and cooling devices. Such effort has been made to use nanofluids in two-phase boiling systems, single-phase convective processes and microelectronic cooling systems together with studies related to the heat pipes working with nanofluids. Majority of these studies have come up with an anomalous enhancement in heat transfer coefficient, followed by negligible pumping power. For example, Zhou *et al.* [22] investigated the potential of graphene oxide nanofluid in an oscillating heat pipe at various concentration of graphene oxide and different power throughputs. They found that at appropriate filling ratios of 55%, 62%, and 70%, the thermal resistance of the system drops by 83.6% compared to the deionized water. Kavusi *et al.* [23] developed a two-dimensional numerical model to assess the performance of a heat pipe working with different nanofluids. They assessed alumina, copper oxide, and silver nanoparticles at different concentrations. They noticed that utilisation of nanofluid decreased the axial-flow pressure of the fluid inside the wick, facilitating the heat transfer inside the heat pipe. Pise *et al.* [24] conducted a set of experiments to study the potential influence of nanofluid on the thermal performance of a thermosiphon heat pipe. They chose alumina/water nanofluid together with the surfactant and studied the influence of coolant rate, concentration of nanomaterial on the performance of the heat pipe. It was found that 50 deg of tilt angle, the thermal performance of the heat pipe was maximised in comparison with water. Also, the performance of heat pipe increased with an increase in the mass concentration of the working fluid inside the heat pipe. Cieslinski tested the performance of a heat pipe working with distilled water and water/alumina nanofluid [25]. Nanoparticles were tested at the concentration of 0.01% and 0.1% by weight. A modified Peclet equation and Wilson method were used to estimate the overall heat transfer coefficient of the

heat pipe. The obtained results indicate better performance of the heat pipe with nanofluids as working fluid in comparison with the base fluid, independent of nanoparticle concentration tested. Noie *et al.* [26] tested the performance of a thermosiphon working with alumina/water nanofluid and showed that the efficiency of the heat pipe can be improved up to 14.7% in comparison with the case in which pure water was used as the working fluid. Also, the temperature profile for the nanofluid was lower than pure water showing lower thermal resistance. For most of the single-phase studies in which heat pipe is not under high heat flux condition, the thermal performance of the heat pipe is enhanced by adding the nanoparticles.

However, for two phase studies, the deposition of nanoparticles on the surface seemed to be a bit challenging. In a two-phase system, the layer of nanofluid close to the heating surface severely experiences a two-phase condition. This is because the microlayer around the surface reaches the base fluid boiling temperature. Hence, bubbles form and the microlayer becomes more concentrated in terms of nanoparticles [27,28]. In this condition, the force balance between attractive-repulsive forces inside the base fluid changes resulting in the separation of nanoparticles and the creation of fouling layer on the surface. Such fouling layer changes the irregularities and microcavities of the surface decreasing the bubble behaviour and a reduction in the rate of bubble formation [29]. Furthermore, the stability of nanofluid plays a major role here, which can change the behaviour of nanoparticles significantly [30].

If a nanofluid can represent longer stability at temperatures close to the base fluid boiling temperature, the aforementioned challenges can be avoided. In the present work, a new nanofluid is introduced which not only provides better thermal stability, but also can work in the boiling heat transfer region, while showing a better particle–fluid interaction. Acetone is a well-known working fluid with a long history of use in heat pipes and thermosiphons. The low tolerance against high temperature (boiling temperature is 56 °C) is kind of advantage for this fluid to be used in a heat pipe [31]. Hence, in the present work, acetone is used with the view to enhance the performance of evaporation of the nanofluid inside the heat pipe. Zirconia is used as conductive solid nanoparticles which are dispersed in the acetone to increase its thermal conductivity and heat capacity. Influence of different operating parameters such as heat flux applied to evaporator, mass concentration of zirconia nanoparticles, the filling ratio and tilt angle of the heat pipe on the heat transfer coefficient of heat pipe and its thermal

resistance is investigated. The optimum value for the tilt angle and filling ratio was also obtained.

2 Experimental

2.1 Experimental setup

Figure 1 presents a schematic diagram of the experimental setup used in the present research. The heart of the setup was a heat pipe fabricated from oxygen-free copper. The heat pipe was fabricated from copper with diameter of 15 mm and evaporator-condenser length of 100 mm and adiabatic length of 50 mm. The middle section of the heat pipe was heavily insulated with glass wool to provide a sufficient insulation for the adiabatic region. The evaporator section was covered with a flexi spring heater (manufactured by 3M Co.) to provide the required heat flux to the system. The condenser section is cooled with a stainless steel water jacket connected to a refrigerant-based thermostat bath. The temperature of the condenser was set at 20 °C and its temperature was monitored constantly using a K-type thermocouple (accuracy: ±0.1 K, manufactured by Omega Eng.). To ensure that the thermal resistance of the system is minimised, silicon paste (with thermal conductivity of 5 W/(mK)) was injected inside the thermowells, which not only removes the air from the thermowells, but also provides a conductive medium around the thermocouples and reduces the thermal resistance. To obtain the temperature distribution (thermal profile), three K-type thermocouples were mounted on the evaporator section, two for the adiabatic and three for the condenser section to constantly monitor the temperature of the heat pipe. All thermocouples were connected to a data logger (frequency: 1 kHz, manufactured by National Instruments) connected to a personal computer (PC). To charge the heat pipe, a syringe pump was used to accurately fill the heat pipe with nanofluid, while a micro vacuum pump was used to remove air from the heat pipe. To provide different tilt angles to the heat pipe, a movable base was designed in a way to provide the conditions to fix the heat pipe at different tilt angles. A vibration-protected table was employed to eliminate any effects of vibration of table or facilities on the heat pipe. The inclination and tilt angle of the heat pipe was measured using the inclinometer manufactured by Kawasaki Co. Notably, all the thermocouples, inclinometer, heater and data logger were calibrated, tested and validated to ensure the accuracy and reliability of the data. Also, measurements were performed three times

to ensure the repeatability and reproducibility. Notably, we assessed the heat loss from the evaporator and also from the condenser. An energy balance was conducted between the input heat through evaporator and the convective heat to environment and a deviation of 5.3% was obtained.

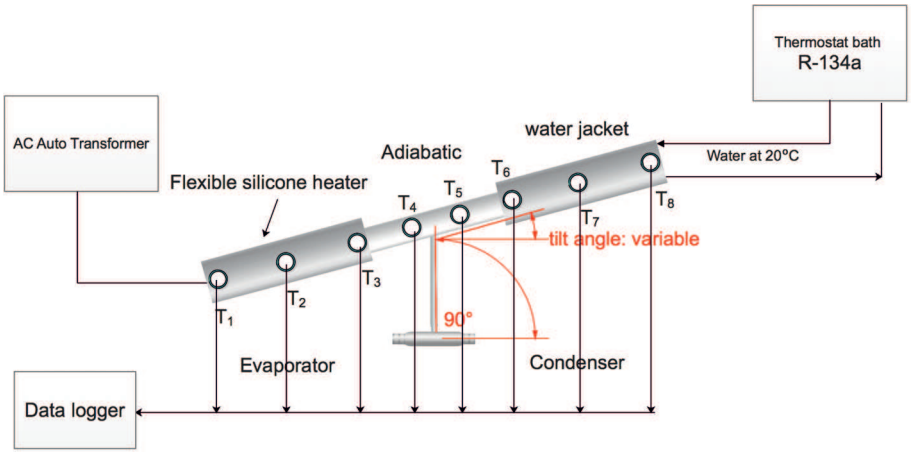

Figure 1: Experimental setup used in the present research (T_1 – T_3 are evaporator's temperature, T_4–T_5 are adiabatic and T_6–T_8 are condenser temperature).

2.2 Preparation of the working fluid

To prepare the nanofluids, zirconia nanoparticles were purchased and used. The nominal size of the nanoparticles was approximately 50 nm, which was later confirmed by scanning the electron microscopic images. To disperse the nanofluids, a two-step method was used represented in Fig. 2a. Initially, the base fluid was prepared by adding acetone to ethylene glycol (a mixture of 40:60 by volume). Then, the desired weight of nanoparticles was added to the base fluid and a 40 kHz, 400 W sonication probe was utilised to further disperse the nanoparticles within the base fluid. To maintain a longer stability, nonylphenol ethoxilate was added to the nanofluid at 0.1% of general volume of the nanofluid together with a pH refinement ensuring the zeta potential of the nanofluid is higher than 20 mV. A zeta sizer was used to measure the zeta potential of the nanofluid. Since, the stability tests were time-consuming, a central composite design (CCD) [38], a well-known technique of response surface methodology was used to reduce the number of iterations and optimise the longest stability of the nanofluid. Table 1 presents the optimised conditions applied to obtain the longest stability.

Table 1: Iterations and the optimised conditions for the stability of acetone/ethylene glycol-based nanofluids.

Concentration [%]	Stirring [min]	pH refinement [–]	Zeta potential [mV]	Sonication [min]	Surfactant [%]	Stability [week]
0.05	10	yes, 7.4	-23	10	0.1	2
0.10	15	yes, 7.8	-24.5	12	0.1	2
0.15	20	yes, 8.1	-27.2	12	0.1	> 2

Notably, this range of concentration was selected since the stability of the nanoparticles within the base fluid can be maintained. For larger concentration, the nanofluid starts forming a deposition layer inside the pipes and also the system. Also, in this range of concentration, the change in thermal performance of the systems was tangible. Together with zeta potential and pH refinement, a time-settlement visualization was performed to ensure that the nanofluids are stable. Hence, nanofluids were loaded into a glass-made container and the sedimentation layer of nanoparticles at the bottom of the container was monitored. The obtained results shown in Tab. 1 were in accordance with the visualization assessment. Figure 2b presents the prepared nanofluids after the stability treatment. Figure 2c, also shows the morphology and size of the zirconia nanoparticles. The mean size of the particles was 25 nm.

2.3 Data reduction and uncertainty

To calculate the thermal resistance and heat transfer coefficient of the heat pipe, following equations were used:

$$R = \frac{T_e - T_c}{Q} \,, \tag{1}$$

were T_e and T_c are the mean value of the temperatures measured for the evaporator section and also for the condenser section. To calculate the heat transfer coefficient (HTC), heat flux needs to be estimated. To do so, the following expression was used to calculate the thermal load to the evaporator

$$Q = IV \,, \tag{2}$$

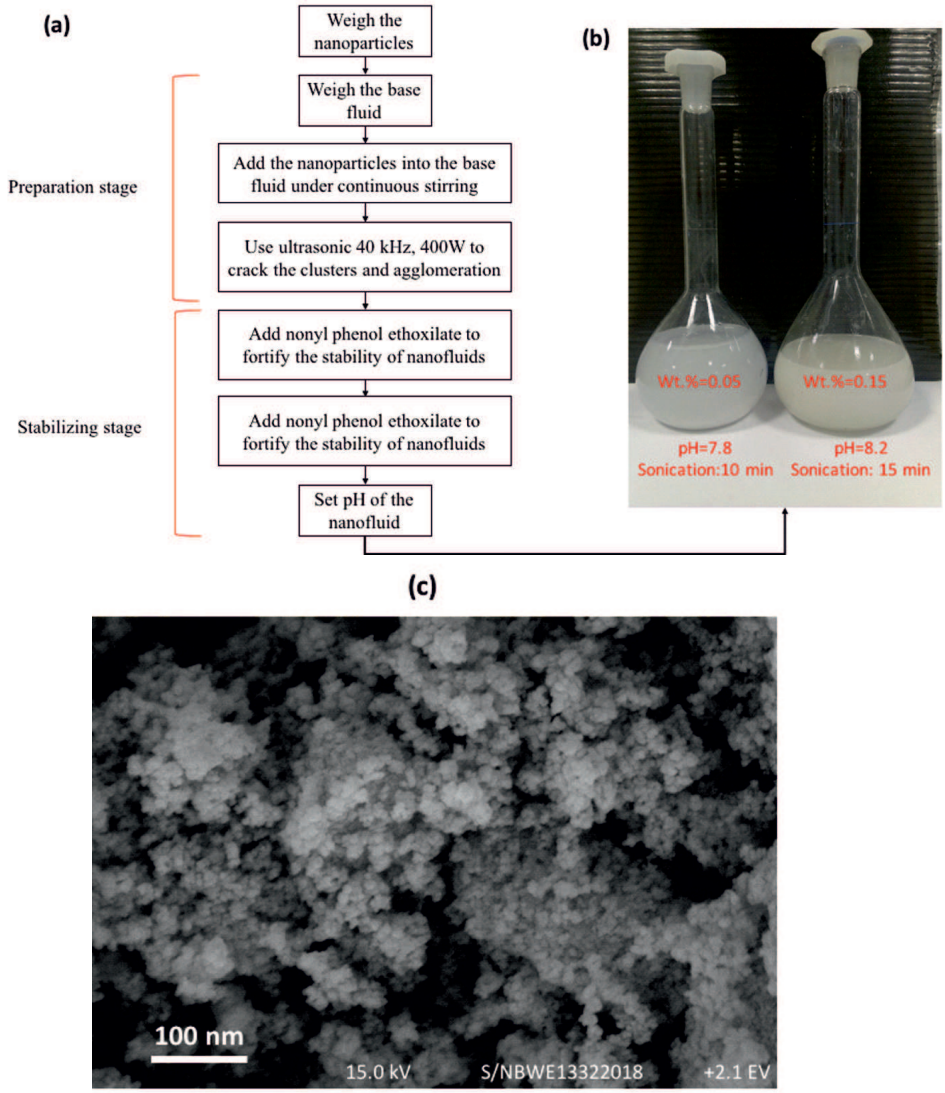

Figure 2: (a) The schematic diagram of the preparation method for nanofluids, (b) sample of a stable nanofluid after 14 days, (c) scanning electron microscopic image taken from zirconia nano-powder.

.

where V, is the voltage of the silicone heater and I is the current passing through the silicone heater. The HTC of the evaporator section is calculated by the following equation:

$$h_e = \frac{q_e}{\Delta T_e} , \tag{3}$$

where ΔT_e is the temperature difference between the evaporator and the adiabatic sections since the heat transfer coefficient is defined for the evaporator section and

$$q_e = \frac{Q}{\pi D L} . \tag{4}$$

Here $L = 100$ mm is the length of the evaporator section and $D = 15$ mm is the diameter of the heat pipe.

Filling ratio and tilt angle are the two key operating parameters which are assessed in the present research. Filling ratio is also defined as the volume of the working fluid to the total volume of the heat pipe. Tilt angle is also defined as the angle between the heat pipe and the horizontal line.

Table 2: Uncertainty of measurement instruments.

Parameter	Unit	Instrument	Uncertainty
Voltage of the heater	V	Multimeter (Fluke)	±0.01
Current passing through the heater	A	Multmeter (Fluke)	±0.02
Temperature	K	Thermocouple K-type (Omega)	±0.02
Tilt angle	deg	Inclinometer (Kawasaki)	±0.1

Table 2 expresses the accuracy of the devices and measurement instruments used in the present research. The uncertainties of some operating parameters including the temperature of heat pipe, the voltage and current of the heater are system-related parameters (e_s), while the random uncertainty (e_r) can be obtained with measuring of the heat loss, repeatability and reproducibility [32]. The overall uncertainty of the tests can be calculated using the following equation [33]:

$$e = \sqrt{e_s^2 + e_r^2} . \tag{5}$$

Thereby, the overall uncertainty for the thermal resistance measurement was 8.2%, for heat transfer coefficient was 11.1% and for heat loss was 7.2%.

3 Results and discussion

3.1 Temperature profile

Figure 3 presents the variation of temperature of the heat pipe with the axial distance from the tip of heat pipe (tip of the evaporator section) for two different power throughputs. As can be seen, the temperature profile is highest in the evaporator section and is the lowest in condenser section, which is attributed to the presence of the silicone heater in the evaporator section and also the cooling jacket mount on the condenser section. Temperature slightly decreased from the evaporator to adiabatic region and suddenly drops from adiabatic section to the condenser section. In adiabatic region, since insulation prevents the convective loss to environment, most of the heat is directly transferred to the condenser part. In the condenser section, due to the convective heat transfer between the working fluid and the condenser cooling liquid, the temperature significantly drops. For example, at $Q = 70$ W, the average temperature of the evaporator section for nanofluid at 0.05% wt. is about 65 °C, while for the adiabatic and condenser sections, temperature reaches approximately 58 °C and 22 °C. Interestingly, with an increase in the mass concentration of the nanofluids, the temperature profile of the heat pipe decreases, which is attributed to the thermal resistance of the heat pipe. For nanofluids at larger mass concentration of nanoparticles, the thermal resistance of the heat pipe decreases. This is because, the presence of nanoparticles within acetone intensifies the thermal characteristics of the working fluid. Nanoparticles add Brownian motion and thermophoresis to the base fluid resulting in a better local movement, heat transport and thermal conductivity over the base fluid (here, acetone). Hence, nanoparticle suppress the thermal resistance of the heat pipe, and as a result increase the heat transfer inside the evaporator and even condenser. Overall, presence of nanoparticles enhanced the thermal performance of the heat pipe. The maximum reduction in temperature profile belonged to the nanofluid at 0.15% wt. which was approx. 9.8% in comparison with 0.05% wt. and 19.8% in comparison with the pure acetone (which has not been plotted in the figure). The same trend was also seen for other heat loads such as $Q = 30$ W as represented in Fig. 3b. Notably, the temperature of the condenser was set at 20 °C using a thermostat bath working with R134a/R136a refrigerant mixture as a working fluid.

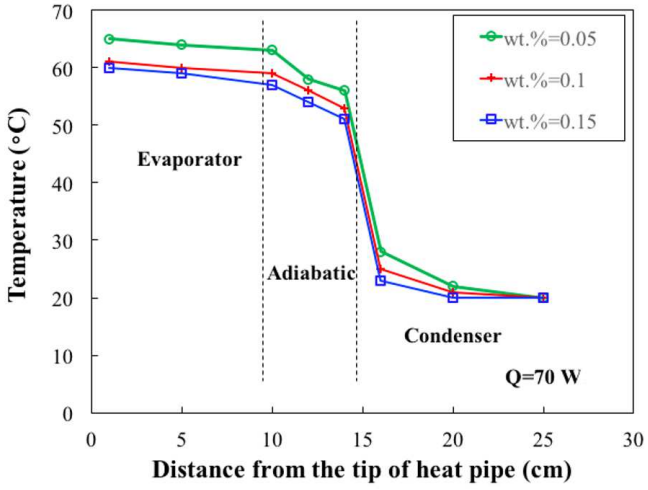

(a)

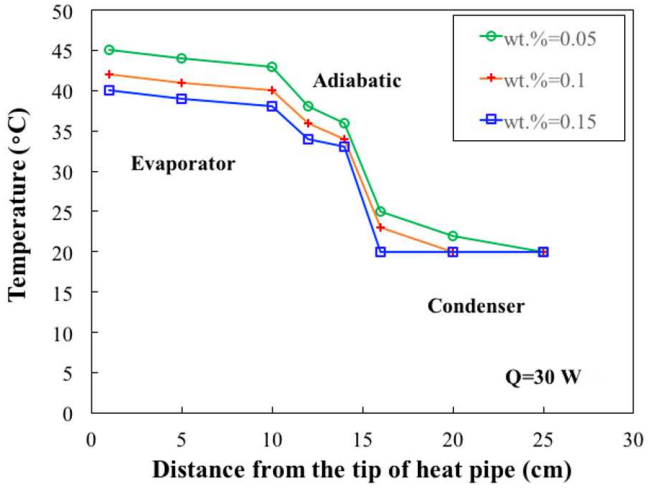

(b)

Figure 3: Variation of the temperature of heat pipe with axial distance from the tip of the heat pipe and for two different heat loads: (a) $Q = 70$ W, (b) $Q = 30$ W.

3.2 Filling ratio

Figure 4 presents the variation of heat transfer coefficient of heat pipe in evaporator section with filling ratio and for various mass concentration of nanofluids. As can be seen, with an increase in the value of filling ratio, the

heat transfer coefficient nonlinearly increases reaching an optimum point after which the heat transfer coefficient decreases with an increase in the filling ratio. This is because, heat pipe's volume is the key characteristics which can limit the movement of the working fluid. In fact, there are two main parameters determining the increase and/or decrease of the heat transfer coefficient: 1) interaction between vapour and liquid phase in the heat pipe and 2) pressure drop due to the evaporation of working fluid. When the value of filling ratio increases to a specific value (here, 0.65), the heat pipe is more filled with liquid working fluid, hence, lower space remains for the migration of evaporated working fluid. Also, this limitation results in the change in the internal pressure of the heat pipe. In the evaporator, more acetone is evaporated, while there is no enough space to migrate to the condenser. Hence, the pressure in the evaporator goes higher, while pressure in the condenser is still low. Since space is not sufficient for the movement of the evaporated working fluid, the microconvective vaporised streams are captured by the liquid working fluid. Hence, heat transfer coefficient decreases. Interestingly, with an increase in the mass concentration of nanofluid, the heat transfer coefficient increases. This can also be attributed to the increase in the thermal conductivity and decrease in the thermal resistance of the heat pipe. For the present work, the optimised filling ratio was 0.65 for all the mass concentrations of nanofluids.

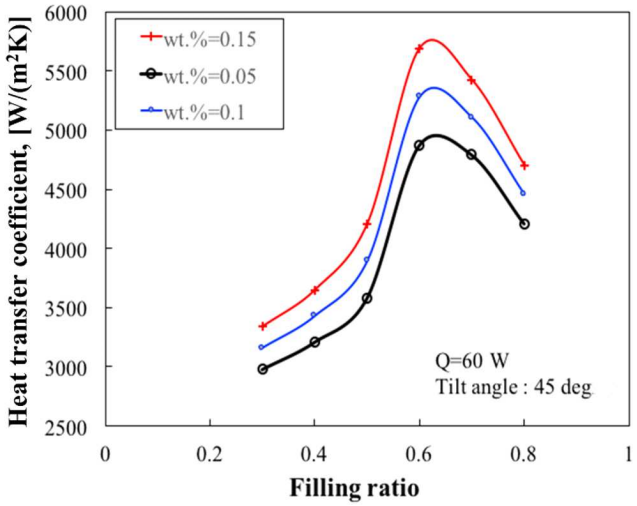

Figure 4: Dependence of heat transfer coefficient of evaporator on the filling ratio of the working fluid and for various mass concentrations of nanofluids.

3.3 Tilt angle

Figure 5 presents the variation of heat transfer coefficient with the tilt angle of the heat pipe and for various mass concentrations of nanofluid. As

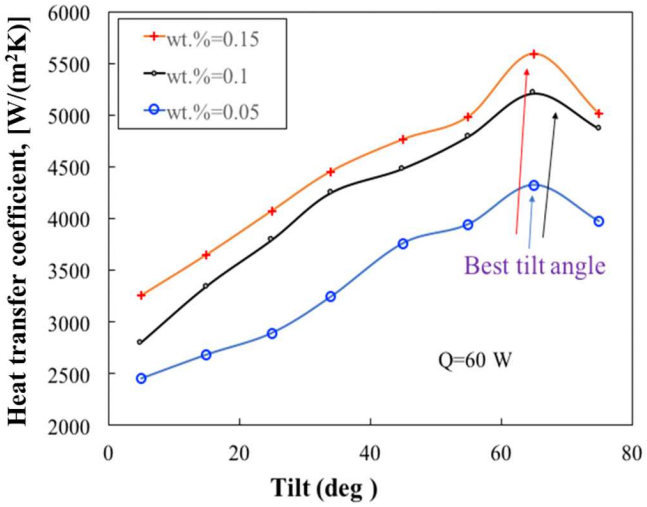

Figure 5: Dependence of heat transfer coefficient of evaporator on the tilt angle of the working fluid and for various mass concentrations of nanofluids.

can be seen, with an increase in the tilt angle of the heat pipe, the heat transfer coefficient increases. For example, for nanofluid at 0.05% wt. and at a tilt angle of 25 degree, the HTC is approx. 2700 W/(m^{2}K), while it is 4100 W/(m^{2}K) at a tilt angle of 65 deg. This enhancement can be attributed to the positive influence of gravity which facilitates returning of the working fluid from the condenser to the evaporator section. The faster the working fluid is returned to evaporator, the better thermal performance and heat transfer coefficient can be achieved. Also, due to the presence of nanoparticles, the Brownian motion of the particles enhances the heat transfer within the heat pipe. The local agitation and movement of the nanoparticles provide better liquid-solid contacts and as a result, at larger tilt angles, higher Brownian motion is achieved due to the gravity-assisted velocity and higher HTC is obtained. However, from a specific tilt angle, the working fluid is entrained in the evaporator section and heat transfer in the evaporator is suppressed. Thereby, there is a trade-off between the tilt angle and also the heat transfer coefficient. Furthermore, there is an optimum point (here 60–65 deg), in which the maximum heat transfer coefficient can

be achieved. For all the concentrations of nanofluids and for all heat loads, the same behaviour was seen.

3.4 Applied heat flux to the evaporator

Figure 6 presents the dependence of heat transfer coefficient on the applied heat flux for various mass concentrations of nanofluid at a tilt angle of 55 deg. As can be seen, with an increase in the applied heat flux, the heat transfer coefficient significantly increases and the trend of increase in nonlinear. Two main heat transfer domains can be identified. In the first domain in which heat flux is lower than 25 kW/m^2, the convective heat transfer is the main domain of heat transfer, while for the larger heat fluxes, due to rapid evaporation and considering the boiling temperature of acetone (56 °C), the nucleate boiling heat transfer is the main domain of heat transfer. Hence, the heat transfer coefficient in the second domain is several times larger than that measured for the convective domain. This is because, in the boiling heat transfer region, the bubbles are formed and the local agitation due to the bubble interactions drastically elevates the heat transfer coefficient. This has already been shown in the literature [34–37].

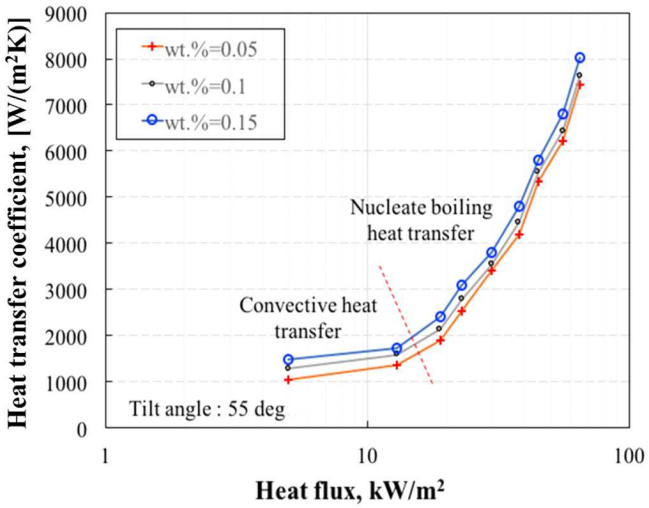

Figure 6: Dependence of heat transfer coefficient of evaporator on the applied heat flux and for various mass concentrations of nanofluids.

Also, due to the presence of nanoparticles, a porous layer of deposition can be formed on the internal wall of the heat pipe, which increases the nucle-

ation and bubble formation inside the heat pipe. Hence, zirconia/acetone nanofluid is a promising working fluid for high heat flux cooling regimes. In fact, the presence of particles can intensify the nucleate boiling heat transfer resulting in the massive removal of heat from the evaporator section. As can also be seen, the highest heat transfer coefficient belongs to nanofluid at 0.15% wt., and this can be seen for all domains and for any values of tilt angle or filling ratios.

3.5 Thermal resistance

Figure 7 presents the dependence of thermal resistance of the heat pipe on the applied heat flux for various mass concentrations of nanofluid.

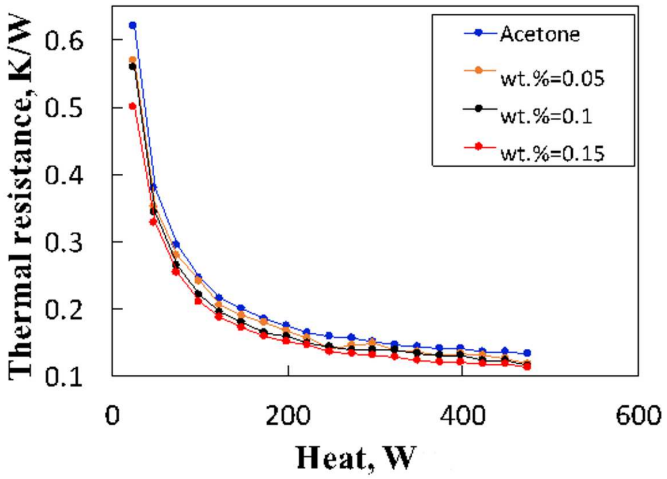

Figure 7: Dependence of thermal resistance of the evaporator on the applied heat flux and for various mass concentrations of nanofluids.

As can be seen, with an increase in the applied heat flux, the thermal resistance of the heat pipe decreases. This can be attributed to the change in the mechanism of heat transfer from convective to nucleate boiling mechanism. Interestingly, with an increase in the nanoparticle's concentration, the thermal resistance of the heat pipe decreases, which is due to the increase in thermal conductivity of the working fluid, Brownian motion and thermophoresis phenomena which all intensify the heat transfer and decrease the heat pipe thermal resistance. The minimum thermal resistance belonged to nanofluid at wt. 0.15% wt., which was 0.12 K/W, while for

the same heat flux, the thermal resistance was 0.16 K/W and 0.13 K/W for 0.05% wt. and 0.1% wt.. Hence, the presence of nanoparticles offers a potential to decrease the thermal resistance of the heat pipe, which in turn increases the thermal performance of the device. Notably, the average thermal fouling resistance measured for the nanofluids at 0.05% wt., 0.1% wt., and 0.15% wt. was 0.3 K/W, 0.37 K/W, and 0.675 K/W, respectively.

4 Conclusion

An experimental investigation was conducted on the thermal performance of a rod heat pipe working with zirconia/acetone nanofluid and following conclusions were obtained:

- The presence of zirconia nanoparticles decreased the temperature profile of the heat pipe and the maximum reduction in temperature belonged to 0.15% wt.
- An increase in the heat flux applied to the evaporator resulted in the increase in heat transfer coefficient of the heat pipe. Also, the presence of zirconia nanoparticles intensified the heat transfer coefficient. The maximum heat transfer coefficient belonged to the heat pipe working with nanofluid at 0.15% wt. and filling ratio of 0.65 and tilt angle of 60–65 deg.
- Filling ratio was found to initially increase the heat transfer coefficient due to the increase in the number of nanoparticles inside the heat pipe, however, from a specific value of 0.65, due to the limitation in the internal space of the heat pipe, the heat transfer coefficient was deteriorated.
- For the tilt angle, with an increase in the tilt angle of the heat pipe, the heat transfer coefficient initially increases, from a specific degree (60-65 deg) due to the accumulation of the working fluid inside the heat pipe, the surface contact with evaporator decreases and as a result the heat transfer coefficient decreases for higher tilt angles.

Overall, zirconia/acetone showed a great thermal performance inside the rod heat pipe. However, further research is still required to test this working fluid under various operating conditions with the view to better understand its behaviour.

Acknowledgment The authors of this work tend to appreciate Yazd University for their financial supports.

Received 4 October 2018

References

[1] Faghri A.: *Heat pipes: review, opportunities and challenges*. Fr. Heat Pipes (FHP) **5**(2014), 1, 1–48.

[2] Reay D., McGlen R., Kew P.: *Heat Pipes: Theory, Design and Applications*. Butterworth-Heinemann, Waltham 2013.

[3] Faghri A.: *Review and advances in heat pipe science and technology*. J. Heat Transfer **134**(2012), 12, 123001

[4] Sarafraz M., Hormozi F.: *Experimental study on the thermal performance and efficiency of a copper made thermosyphon heat pipe charged with alumina–glycol based nanofluids*. Powder Technol. **266**(2014), 378–387.

[5] Nakhjavani M., Nikkhah V., Sarafraz M., Shoja S., Sarafraz M.: *Green synthesis of silver nanoparticles using green tea leaves: Experimental study on the morphological, rheological and antibacterial behaviour*. Heat Mass Transfer **53**(2017), 10, 3201–3209.

[6] Sarafraz M., Hormozi F., Silakhori M., Peyghambarzadeh S.: *On the fouling formation of functionalized and non-functionalized carbon nanotube nano-fluids under pool boiling condition*. App. Therm. Eng. **95**(2016), 433–444.

[7] Sarafraz M.M., Peyghambarzadeh S.M.: *Experimental study on subcooled flow boiling heat transfer to water–diethylene glycol mixtures as a coolant inside a vertical annulus*. Exp. Therm. Fluid Sci. **50**(2013), 154–162.

[8] Sarafraz M., Hormozi F.: *Forced convective and nucleate flow boiling heat transfer to alumnia nanofluids*. Period. Polytech. Chem. **58**(2014), 1, 37–46.

[9] Sarafraz M.M., Safaei M.R.: *Diurnal thermal evaluation of an evacuated tube solar collector (ETSC) charged with graphene nanoplatelets-methanol nanosuspension*. Renew. Energ. **142**(2019), 364-372.

[10] Nakhjavani M., Nikounezhad N., Ashtarinezhad A., Shirazi F.H.: *Human lung carcinoma reaction against metabolic serum deficiency stress*. Iran J. Pharm. Res. (IJPR) **15**(2016), 4, 817–823.

[11] Nakhjavani M., Stewart D., Shirazi F.: *Effect of steroid and serum starvation on a human breast cancer adenocarcinoma cell line*. J. Exp. Ther. Oncol. **12**(2017), 1, 25–34.

[12] Nakhjavani M., Vatanpour H., Shahriari F., Mohamadzadehasl B.: *Life-saving effect of lidocaine on Odontobuthos Doriae scorpion envenomation in mice*. Am. J. PharmTech Res. **6**(2016), 5, 179–190.

[13] Nikounezhad N., Nakhjavani M., Shirazi F.: *Cellular glutathione level does not predict ovarian cancer cells' resistance after initial or repeated exposure to cisplatin*. J. Exp. Ther. Oncol. **12**(2017), 1, 1–7.

[14] Shirazi F.H., Zarghi A., Kobarfard F., Zendehdel R., Nakhjavani M., Arfaiee S., Zebardast T., Mohebi S., Anjidani N., Ashtarinezhad A.: *Remarks in successful cellular investigations for fighting breast cancer using novel synthetic compounds*. In: Breast Cancer-Focusing Tumor Microenvironment, Stem cells and Metastasis (M. Gunduz, Ed.), InTech, 2011.

[15] Sarafraz M.M., Hormozi F., Kamalgharibi M.: *Sedimentation and convective boiling heat transfer of CuO-water/ethylene glycol nanofluids*. Heat and Mass Transfer **50**(2014), 9, 1237–1249.

[16] Pourmehran O., Sarafraz M.M., Rahimi-Gorji M., Ganji D.D.: *Rheological behaviour of various metal-based nano-fluids between rotating discs: a new insight*. J. Taiwan Inst. Chem. E. **88**(2018), 37–48.

[17] Tabassum R., Mehmood R., Pourmehran O., Akbar N., Gorji-Bandpy M.: *Impact of viscosity variation on oblique flow of Cu–H_2O nanofluid*. P. I. Mech. Eng. E-J. PRO. **232**(2018), 5, 622–631.

[18] Yousefi M., Pourmehran O., Gorji-Bandpy M., Inthavong K., Yeo L., Tu J.: *CFD simulation of aerosol delivery to a human lung via surface acoustic wave nebulization*. Biomech. Model. Mechan. **16**(2017), 6, 2035–2050.

[19] Yu W., France D.M., Routbort J.L., Choi S.U.: Review and comparison of nanofluid thermal conductivity and heat transfer enhancements. Heat Transfer Eng. **29**(2008), 5, 432–460.

[20] Yu W., France D.M., Choi S.U., Routbort J.L.: *Review and Assessment of Nanofluid Technology for Transportation and Other Applications*. Argonne National Laboratory, ANL/ESD/07-9, 2007.

[21] Verma S.K., Tiwari A.K.: *Progress of nanofluid application in solar collectors: A review*. Energ. Convers. Manage. **100**(2015), 324–346.

[22] Zhou Y., Cui X, Weng J., Shi S., Han H., Chen C.: *Experimental investigation of the heat transfer performance of an oscillating heat pipe with graphene nanofluids*. Powder Technol. **332**(2018), 371–380.

[23] Kavusi H., Toghraie D.: *A comprehensive study of the performance of a heat pipe by using of various nanofluids*. Adv. Powder Technol. **28**(2017), 11, 3074–3084.

[24] Pise G.A., Salve S.S., Pise A.T., Pise A.A.: *Investigation of solar heat pipe collector using nanofluid and surfactant*. Energy Proced. 90(2016). 481–491.

[25] Cieśliński J.T.: *Effect of nanofluid concentration on two-phase thermosyphon heat exchanger performance*. Arch. Thermodyn. **37**(2016), 2, 23–40.

[26] Noie S., Heris S.Z., Kahani M., Nowee S.: *Heat transfer enhancement using Al_2O_3/water nanofluid in a two-phase closed thermosyphon*. Int. J. Heat Fluid Fl. 30(2009), 4, 700–705.

[27] Judd R., Hwang K.: *A comprehensive model for nucleate pool boiling heat transfer including microlayer evaporation*. J. Heat Trans. **98**(1976), 4, 623–629.

[28] Cooper M., Lloyd A.: *The microlayer in nucleate pool boiling*. Int. J. Heat Mass Tran. **12**(1969), 8, 895–913.

[29] Kim H.D., Kim M.H.: *Effect of nanoparticle deposition on capillary wicking that influences the critical heat flux in nanofluids*. Appl. Phys. Lett. **91**(2007), 014104.

[30] Sarafraz M.M., Arjomandi M.: *Thermal performance analysis of a microchannel heat sink cooling with copper oxide-indium (CuO/In) nano-suspensions at high-temperatures.* Appl. Therm. Eng. **137**(2018), 700–709.

[31] Abhat A., Seban R.: *Boiling and evaporation from heat pipe wicks with water and acetone.* J. Heat Trans. 96(1974), 3, 331–337.

[32] Kline S.J., McClintock F.A.: *Describing uncertainties in single-sample experiments.* Mech. Eng. **75**(1953), 1, 3–8.

[33] Moffat R.J.: *Using uncertainty analysis in the planning of an experiment.* J. Fluids Eng. 107(1985), 2, 173–178.

[34] Sarafraz M.M., Arya A., Nikkhah V., Hormozi F.: *Thermal performance and viscosity of biologically produced silver/coconut oil nanofluids.* Chem. Biochem. Eng Q. **30**(2016), 4, 489–500.

[35] Sarafraz M.M.: *Experimental investigation on pool boiling heat transfer to formic acid, propanol and 2-butanol pure liquids under the atmospheric pressure.* J. Appl. Fluid Mech. **6**(2013), 1, 73–79.

[36] Sarafraz M.M., Arjomandi M.: *Demonstration of plausible application of gallium nano-suspension in microchannel solar thermal receiver: experimental assessment of thermo-hydraulic performance of microchannel.* Int. Commun. Heat Mass **94**(2018), 39–46.

[37] Sarafraz M., Peyghambarzadeh S.: *Influence of thermodynamic models on the prediction of pool boiling heat transfer coefficient of dilute binary mixtures.* International Commun. Heat Mass Transf. **39**(2012), 8, 1303–1310.

[38] Chiang K.T., Chou C.C., Liu N.M.: *Application of response surface methodology in describing the thermal performances of a pin-fin heat sink.* Int. J. Therm. Sci. **48**(2009), 6, 1196–205.